

Testing $SO(10)$ -inspired leptogenesis with low energy neutrino experiments

Pasquale Di Bari^{a,b} and Antonio Riotto^{c,d}

^a *School of Physics and Astronomy, University of Southampton, Southampton, SO17 1BJ, U.K.*

^b *Department of Physics and Astronomy, University of Sussex, Brighton, BN1 9QH, U.K.*

^c *INFN, Sezione di Padova, Dipartimento di Fisica Galileo Galilei*

Via Marzolo 8, I-35131 Padua, Italy

^d *CERN, PH-TH Division, CH-1211, Geneva 23, Switzerland*

July 23, 2013

Abstract

We extend the results of a previous analysis of ours showing that, when both heavy and light flavour effects are taken into account, successful minimal (type I + thermal) leptogenesis with $SO(10)$ -inspired relations is possible. Barring fine tuned choices of the parameters, these relations enforce a hierarchical RH neutrino mass spectrum that results into a final asymmetry dominantly produced by the next-to-lightest RH neutrino decays (N_2 dominated leptogenesis). We present the constraints on the whole set of low energy neutrino parameters. Allowing a small misalignment between the Dirac basis and the charged lepton basis as in the quark sector, the allowed regions enlarge and the lower bound on the reheating temperature gets relaxed to values as low as $\sim 10^{10}$ GeV. It is confirmed that for normal ordering (NO) there are two allowed ranges of values for the lightest neutrino mass: $m_1 \simeq (1 - 5) \times 10^{-3}$ eV and $m_1 \simeq (0.03 - 0.1)$ eV. For $m_1 \lesssim 0.01$ eV the allowed region in the plane θ_{13} - θ_{23} is approximately given by $\theta_{23} \lesssim 49^\circ + 0.65(\theta_{13} - 5^\circ)$, while the neutrinoless double beta decay effective neutrino mass falls in the range $m_{ee} = (1 - 3) \times 10^{-3}$ eV for $\theta_{13} = (6^\circ - 11.5^\circ)$. For $m_1 \gtrsim 0.01$ eV, one has quite sharply $m_{ee} \simeq m_1$ and an upper bound $\theta_{23} \lesssim 46^\circ$. These constraints will be tested by low energy neutrino experiments during next years. We also find that inverted ordering (IO), though quite strongly constrained, is not completely ruled out. In particular, we find approximately $\theta_{23} \simeq 43^\circ + 12^\circ \log(0.2 \text{ eV}/m_1)$, that will be fully tested by future experiments.

1 Introduction

With the discovery of neutrino masses and mixing in neutrino oscillation experiments, leptogenesis [1, 2] has become the most attractive model of baryogenesis to explain the observed matter-antimatter asymmetry of the Universe. This can be expressed for example in terms of the baryon-to-photon number ratio and is very well measured by CMB observations [3] to be

$$\eta_B^{\text{CMB}} = (6.2 \pm 0.15) \times 10^{-10}. \quad (1)$$

Leptogenesis originates from the see-saw mechanism [4] that is based on a simple extension of the Standard Model where right-handed (RH) neutrinos with a Majorana mass matrix M and Yukawa couplings h to leptons and Higgs are added. Within $SO(10)$ models, three RH neutrinos N_i ($i = 1, 2, 3$) are nicely predicted and for this reason they are traditionally regarded as the most appealing theoretical framework to embed the seesaw mechanism.

However, within the simplest set of assumptions inspired by $SO(10)$ models [5], barring strong fine-tuned degeneracies in the RH neutrino mass spectrum and using the experimental information from neutrino oscillation experiments, the traditional N_1 -dominated leptogenesis scenario predicts an asymmetry that falls many orders of magnitudes below the observed one [6, 7]. This is because, within N_1 -dominated leptogenesis, where the spectrum of RH neutrinos is hierarchical and the asymmetry is produced from the decays of the lightest ones, successful leptogenesis implies a stringent lower bound on their mass [8], $M_1 > \mathcal{O}(10^9)$ GeV. On the other hand, $SO(10)$ grand-unified theories typically yield, in their simplest version and for the measured values of the neutrino mixing parameters, a hierarchical spectrum with the RH neutrino masses proportional to the squares of the up-quark masses, leading to $M_1 = \mathcal{O}(10^5)$ GeV and therefore to a final asymmetry much below the observed one.

However, it has been shown [9] that, when the production from the next-to-lightest RH neutrinos [10] and lepton flavour effects [11] are simultaneously taken into account [12], the final asymmetry can be generated by the decays of the next-to-lightest RH neutrinos and allowed regions in the low energy neutrino parameter space open up.

In this paper we proceed with the analysis of [9] and present the resulting constraints on all low energy neutrino parameters. The paper is organized as follows. In Section 2 we discuss the current experimental status on low energy neutrino parameters, we set up the notation and describe the general procedure to calculate the the asymmetry and find the constraints. In Section 3 we first consider the case already studied in [9], when the Dirac basis and the charged lepton basis coincide and then, in Section 4, we allow for a misalignment between the two bases not larger than that one described by the CKM

matrix in the quark sector. Finally, in Section 5 we present a global scan in the space of parameters where all possible cases between the case of no misalignment and the case of a misalignment at the level of the CKM matrix are taken into account. We also discuss two scenarios, one at small m_1 and one at large m_1 , and show how, within $SO(10)$ -inspired models, minimal leptogenesis could be tested in future low energy neutrino experiments.

Notice that our discussion is made within a non-supersymmetric framework. Recently a study of $SO(10)$ -inspired models within a supersymmetric framework has also enlightened interesting potential connections with lepton flavour violating decays and Dark Matter [13]. An analysis of leptogenesis within left-right symmetric models, where a type II seesaw contribution to the neutrino mass matrix is also present, has been performed in [14]. Within these models, the minimal type I scenario considered here represents a particular case recovered under specific conditions.

2 Experimental information and general setup

After spontaneous symmetry breaking, a Dirac mass term $m_D = h v$, is generated by the vacuum expectation value (VEV) $v = 174$ GeV of the Higgs boson. In the see-saw limit, $M \gg m_D$, the spectrum of neutrino mass eigenstates splits in two sets: three very heavy neutrinos, N_1, N_2 and N_3 respectively with masses $M_1 \leq M_2 \leq M_3$ almost coinciding with the eigenvalues of M , and three light neutrinos with masses $m_1 \leq m_2 \leq m_3$, the eigenvalues of the light neutrino mass matrix given by the see-saw formula [4],

$$m_\nu = -m_D \frac{1}{D_M} m_D^T, \quad (2)$$

that we wrote in a basis where the Majorana mass matrix is diagonal defining $D_M \equiv \text{diag}(M_1, M_2, M_3)$. The symmetric light neutrino mass matrix m_ν is diagonalized by a unitary matrix U ,

$$U^\dagger m_\nu U^* = -D_m \quad (3)$$

with $D_m \equiv \text{diag}(m_1, m_2, m_3)$, that, in the basis where the charged lepton mass matrix is diagonal, can be identified with the lepton mixing matrix.

Neutrino oscillation experiments measure two neutrino mass-squared differences. For NO one has $m_3^2 - m_2^2 = \Delta m_{\text{atm}}^2$ and $m_2^2 - m_1^2 = \Delta m_{\text{sol}}^2$. The two heavier neutrino masses can therefore be expressed in terms of the lightest neutrino mass m_1 as

$$m_2 = \sqrt{m_1^2 + m_{\text{sol}}^2}, \quad \text{and} \quad m_3 = \sqrt{m_1^2 + m_{\text{atm}}^2}, \quad (4)$$

where we defined $m_{\text{atm}} \equiv \sqrt{\Delta m_{\text{atm}}^2 + \Delta m_{\text{sol}}^2} = (0.050 \pm 0.001)$ eV and $m_{\text{sol}} \equiv \sqrt{\Delta m_{\text{sol}}^2} = (0.00875 \pm 0.00012)$ eV [15]. Recently, a conservative upper bound on the sum of neutrino

masses, $\sum_i m_i \leq 0.58 \text{ eV}$ (95% CL), has been obtained by the WMAP collaboration [3] combining WMAP 7 years data plus baryon acoustic oscillations observations and the latest HST measurement of H_0 . Considering that it falls in the quasi-degenerate regime, it straightforwardly translates into

$$m_1 < 0.19 \text{ eV} \quad (95\% \text{ CL}). \quad (5)$$

We will adopt the following parametrization for the matrix U in terms of the mixing angles, the Dirac phase δ and the Majorana phases ρ and σ [16]

$$U = \begin{pmatrix} c_{12} c_{13} & s_{12} c_{13} & s_{13} e^{-i\delta} \\ -s_{12} c_{23} - c_{12} s_{23} s_{13} e^{i\delta} & c_{12} c_{23} - s_{12} s_{23} s_{13} e^{i\delta} & s_{23} c_{13} \\ s_{12} s_{23} - c_{12} c_{23} s_{13} e^{i\delta} & -c_{12} s_{23} - s_{12} c_{23} s_{13} e^{i\delta} & c_{23} c_{13} \end{pmatrix} \cdot \text{diag}(e^{i\rho}, 1, e^{i\sigma}) \quad (6)$$

and the following 2σ ranges for the three mixing angles [15]

$$\theta_{12} = (31.3^\circ - 36.3^\circ), \quad \theta_{23} = (38.5^\circ - 52.5^\circ), \quad \theta_{13} = (0^\circ - 11.5^\circ). \quad (7)$$

In the case of IO the expression of m_2 in terms of m_1 becomes

$$m_2 = \sqrt{m_1^2 + m_{\text{atm}}^2 - m_{\text{sol}}^2}, \quad (8)$$

while the expression for m_3 does not change. With the adopted convention for the light neutrino masses, $m_1 < m_2 < m_3$, the case of IO corresponds to relabel the column of the leptonic mixing matrix performing a column cyclic permutation, explicitly

$$U = \begin{pmatrix} s_{13} e^{-i\delta} & c_{12} c_{13} & s_{12} c_{13} \\ s_{23} c_{13} & -s_{12} c_{23} - c_{12} s_{23} s_{13} e^{i\delta} & c_{12} c_{23} - s_{12} s_{23} s_{13} e^{i\delta} \\ c_{23} c_{13} & s_{12} s_{23} - c_{12} c_{23} s_{13} e^{i\delta} & -c_{12} s_{23} - s_{12} c_{23} s_{13} e^{i\delta} \end{pmatrix} \cdot \text{diag}(e^{i\sigma}, e^{i\rho}, 1). \quad (9)$$

The predicted baryon-to-photon ratio η_B is related to the value of the final ($B - L$) asymmetry N_{B-L}^f by [2]

$$\eta_B \simeq 0.96 \times 10^{-2} N_{B-L}^f, \quad (10)$$

where N_{B-L} is the $B - L$ number in a co-moving volume that contains on average one RH neutrino N_i in thermal ultra-relativistic equilibrium abundance ($T \gg M_i$).

The Dirac mass matrix can be diagonalized by a bi-unitary transformation

$$m_D = V_L^\dagger D_{m_D} U_R, \quad (11)$$

where $D_{m_D} = \text{diag}(\lambda_1, \lambda_2, \lambda_3)$. The matrix U_R can be obtained from V_L , U and m_i , considering that it provides a Takagi factorization [17] of [18, 5]

$$M^{-1} \equiv D_{m_D}^{-1} V_L U D_m U^T V_L^T D_{m_D}^{-1}, \quad (12)$$

explicitly

$$M^{-1} = U_R D_M^{-1} U_R^T. \quad (13)$$

For non degenerate M_i , the matrix U_R can be determined noticing that it diagonalizes $M^{-1} (M^{-1})^\dagger$, i.e.

$$M^{-1} (M^{-1})^\dagger = U_R D_M^{-2} U_R^\dagger. \quad (14)$$

This relation determines U_R unless a diagonal unitary transformation, since any $\tilde{U}_R = U_R D_\phi^{-1}$ is also a solution. However, given a \tilde{U}_R , one can fix D_ϕ from the eq. (13),

$$D_\phi = \sqrt{D_M \tilde{U}_R^\dagger M^{-1} \tilde{U}_R^*} \quad (15)$$

and in doing so U_R is unambiguously determined. Inspired by $SO(10)$ relations, we can parameterize the eigenvalues of m_D in terms of the up quark masses as

$$\lambda_1 = \alpha_1 m_u, \quad \lambda_2 = \alpha_2 m_c, \quad \lambda_3 = \alpha_3 m_t. \quad (16)$$

Within $SO(10)$ models one can expect $\alpha_i = \mathcal{O}(1)$ and we will refer to this case. The reader is invited to read Ref. [9] for a more comprehensive discussion about these $SO(10)$ -inspired relations. Notice however that our results will be valid for a much broader range of values, since, quite importantly, it turns out that they are independent of α_1 and α_3 provided $M_3 \gg M_2$ and $M_1 \lesssim 10^9$ GeV. With the parametrization eq. (16) and barring very special choices of parameters where the RH neutrino masses can become degenerate [7]¹, the RH neutrino mass spectrum is hierarchical and of the form (for generic expressions in terms of the low energy parameters, see Ref. [7])

$$M_1 : M_2 : M_3 = (\alpha_1 m_u)^2 : (\alpha_2 m_c)^2 : (\alpha_3 m_t)^2. \quad (17)$$

As we said, the values of α_1 and α_3 are actually irrelevant for the determination of the final asymmetry (unless α_1 is unrealistically large to push M_1 from $\sim 10^5$ GeV above the lower bound $\sim 10^9$ GeV to achieve successful N_1 leptogenesis). On the other hand, the

¹As in [9], we consider only solutions where M_3/M_2 and $M_2/M_1 > 10$. This is clearly a conservative condition, since the asymmetry gets enhanced when $M_2 \simeq M_3$ or $M_2 \simeq M_1$. However, in this way, we only neglect very special points in the parameter space yielding M_3/M_2 and $M_2/M_1 < 10$. We will comment again later on this point.

value of α_2 is relevant to set the scale of the mass $M_2 \simeq 2(\alpha_2 m_c)^2/m_3$ (valid for $\theta_{13} \simeq 0$) of the next-to-lightest RH neutrino mass, but it does not alter other quantities crucial for thermal leptogenesis, such as the amount of wash-out from the lightest RH neutrinos.

Defining the flavoured CP asymmetries as

$$\varepsilon_{2\alpha} \equiv -\frac{\Gamma_{2\alpha} - \bar{\Gamma}_{2\alpha}}{\Gamma_2 + \bar{\Gamma}_2}, \quad (18)$$

these can be calculated using [19]

$$\varepsilon_{2\alpha} \simeq \frac{3}{16\pi(h^\dagger h)_{22}} \left\{ \text{Im} [h_{\alpha 2}^* h_{\alpha 3} (h^\dagger h)_{23}] \frac{\xi(x_3/x_2)}{\sqrt{x_3/x_2}} + \frac{2}{3(x_3/x_2 - 1)} \text{Im} [h_{\alpha 2}^* h_{\alpha 3} (h^\dagger h)_{32}] \right\}, \quad (19)$$

where

$$\xi(x) = \frac{2}{3}x \left[(1+x) \ln \left(\frac{1+x}{x} \right) - \frac{2-x}{1-x} \right] \quad (20)$$

and $\Gamma_{2\alpha}$ is the decay rate of the RH neutrino N_2 into the flavor α with couplings given by the Yukawa's matrix h . We will assume an initial vanishing N_2 -abundance instead of an initial thermal abundance as in [9]. In this way, a comparison of the results in the two analyses gives a useful information about the dependence of the final asymmetry on the initial N_2 abundance when successful leptogenesis is imposed.

Let us now define the flavored decay parameters as

$$K_{i\alpha} = \frac{\Gamma_{i\alpha} + \bar{\Gamma}_{i\alpha}}{H(T = M_i)} = \frac{|(m_D)_{\alpha i}|^2}{m_\star M_i}, \quad (21)$$

where H is the Hubble rate,

$$m_\star = \frac{16 \pi^{5/2} \sqrt{g_\star}}{3\sqrt{5}} \frac{v^2}{M_{\text{Pl}}} \simeq 1.08 \times 10^{-3} \text{ eV}, \quad (22)$$

g_\star is the number of the effective relativistic degrees of freedom and M_{Pl} is the Planck mass. The total decay parameters are then just simply given by $K_i = \sum_\alpha K_{i\alpha}$. It is also convenient to introduce the quantities $P_{2\alpha}^0 = K_{2\alpha}/K_2$.

From the decay parameters one can then calculate the efficiency factors that are the second needed ingredient, together with the CP asymmetries, for the calculation of the final asymmetry. These can be well approximated by the following analytical expression [20]²

$$\kappa(K_2, K_{2\alpha}) = \kappa_-^f(K_2, K_{2\alpha}) + \kappa_+^f(K_2, K_{2\alpha}), \quad (23)$$

²It is in quite a good agreement with the numerical results shown in [21]. The maximum difference is $\sim 30\%$ at the peak for $K_{2\alpha} \sim 1$. For $K_{2\alpha} \gg 1$, the difference is below 10%.

where the negative and the positive contributions are respectively approximately given by

$$\kappa_-^f(K_2, K_{2\alpha}) \simeq -\frac{2}{P_{2\alpha}^0} e^{-\frac{3\pi K_{2\alpha}}{8}} \left(e^{\frac{P_{2\alpha}^0}{2} N_{N_2}(z_{\text{eq}})} - 1 \right), \quad (24)$$

$$N_{N_2}(z_2^{\text{eq}}) \simeq \bar{N}(K) \equiv \frac{N(K_2)}{\left(1 + \sqrt{N(K_2)}\right)^2}, \quad (25)$$

and

$$\kappa_+^f(K_2, K_{2\alpha}) \simeq \frac{2}{z_B(K_{2\alpha}) K_{2\alpha}} \left(1 - e^{-\frac{K_{2\alpha} z_B(K_{2\alpha}) N_{N_2}(z_{\text{eq}})}{2}} \right), \quad (26)$$

where

$$z_B(K_{2\alpha}) \simeq 2 + 4 K_{2\alpha}^{0.13} e^{-\frac{2.5}{K_{2\alpha}}} = \mathcal{O}(1 \div 10). \quad (27)$$

The $SO(10)$ -inspired conditions $\alpha_i = \mathcal{O}(1)$, yield a RH neutrino mass spectrum with $M_1 \ll 10^9 \text{ GeV} \lesssim M_2 \lesssim 10^{12} \text{ GeV} \ll M_3$, though, as we already noticed, this spectrum is obtained for a broader range of α_i values. In this situation, the asymmetry is dominantly produced from N_2 decays at $T \sim M_2$ in a two flavour regime, i.e. when final lepton states can be described as an incoherent mixture of a tauon component and of coherent superposition of a an electron and a muon component. Therefore, at the freeze-out of the N_2 wash-out processes, the produced asymmetry can be calculated as the sum of two contributions,

$$N_{B-L}^{T \sim M_2} \simeq \varepsilon_{2\tau} \kappa(K_2, K_{2\tau}) + \varepsilon_{2e+\mu} \kappa(K_2, K_{2e+\mu}), \quad (28)$$

where $\varepsilon_{2e+\mu}$ stands for $\varepsilon_{2e+\mu} = \varepsilon_{2e} + \varepsilon_{2\mu}$ and $K_{2e+\mu} = K_{2e} + K_{2\mu}$.

More precisely, notice that each flavour contribution to the asymmetry is produced in an interval of temperatures between $M_2/[z_B(K_{2\alpha}) - 2]$ and $M_2/[z_B(K_{2\alpha}) + 2]$, with $\alpha = \tau, e + \mu$.

At $T \lesssim 10^9 \text{ GeV}$ the coherence of the $e + \mu$ quantum states breaks down and a three flavour regime holds, with the lepton quantum states given by an incoherent mixture of e, μ and τ flavours. The asymmetry has then to be calculated at the N_1 wash-out stage as a sum of three flavoured contributions.

The assumption of an initial vanishing N_2 -abundance allows to neglect the phantom terms in the muon and in the electron components [22] so that the final asymmetry can be calculated using the expression

$$N_{B-L}^f \simeq \frac{P_{2e}^0}{P_{2e+\mu}^0} \varepsilon_{2e+\mu} \kappa(K_{2e+\mu}) e^{-\frac{3\pi}{8} K_{1e}} + \frac{P_{2\mu}^0}{P_{2e+\mu}^0} \varepsilon_{2e+\mu} \kappa(K_{2e+\mu}) e^{-\frac{3\pi}{8} K_{1\mu}} + \varepsilon_{2\tau} \kappa(K_{2\tau}) e^{-\frac{3\pi}{8} K_{1\tau}}. \quad (29)$$

Notice that successful leptogenesis relies on points in the parameter space where one out of the three $K_{1\alpha} \lesssim 1$. From this point of view the constraints on low energy neutrino experiments that we will obtain should be quite stable against effects that could enhance the asymmetry such as a resonant enhancement for special points where $(M_3 - M_2)/M_2 \ll 1$. Such effects are however still able to relax the lower bound on M_2 and on the T_{RH} , since the $K_{1\alpha}$'s do not depend on M_2 .

3 The case $V_L = I$

We start from the case $V_L = I$ that has been studied already in [9] deriving constraints in the plane $m_1 - \theta_{13}$ for NO. Here we show constraints on all low energy neutrino parameters, including the case of IO.

3.1 Normal ordering

Let us first discuss the case of NO. In Fig. 1 we plotted the final asymmetry η_B for the same three sets of values of the involved parameters as in the Fig. 4 of Ref. [9], where these three choices were corresponding to three different kinds of solutions for successful leptogenesis. This time the third solution (right panel), is suppressed and successful leptogenesis is not attained. In [9], this was the only solution corresponding to a final asymmetry dominantly in the muon flavour instead than in the tauon flavour (as for the first two). The suppression that we find now is explained partly because we are adopting a correct determination of the phases in the U_R matrix (cf. eq. (15)) and partly because we are now assuming an initial vanishing N_2 -abundance instead than an initial thermal one. We will see however that, allowing for $V_L \neq I$, this kind of solution will again yield successful leptogenesis in some allowed regions of the parameter space, characterized in particular by large values of $m_1 \sim 0.1$ eV.

The solution in the central panel is also partly suppressed and successful leptogenesis is not attained. However, in a parameter scan, we find that this kind of solution can still give successful leptogenesis for slightly different values of the parameters than those indicated in the figure caption. In this case the difference with respect to the results in [9] is explained just in terms of the different assumption on the initial abundance. This dependence on the initial conditions is due to the fact that $K_{2\tau} \sim 1$, i.e. the solution falls in the weak wash-out regime at the production.

Finally, the first solution (left panel) is fully unchanged. It therefore exhibits a full independence of the initial conditions and this is in agreement with the fact that it respects

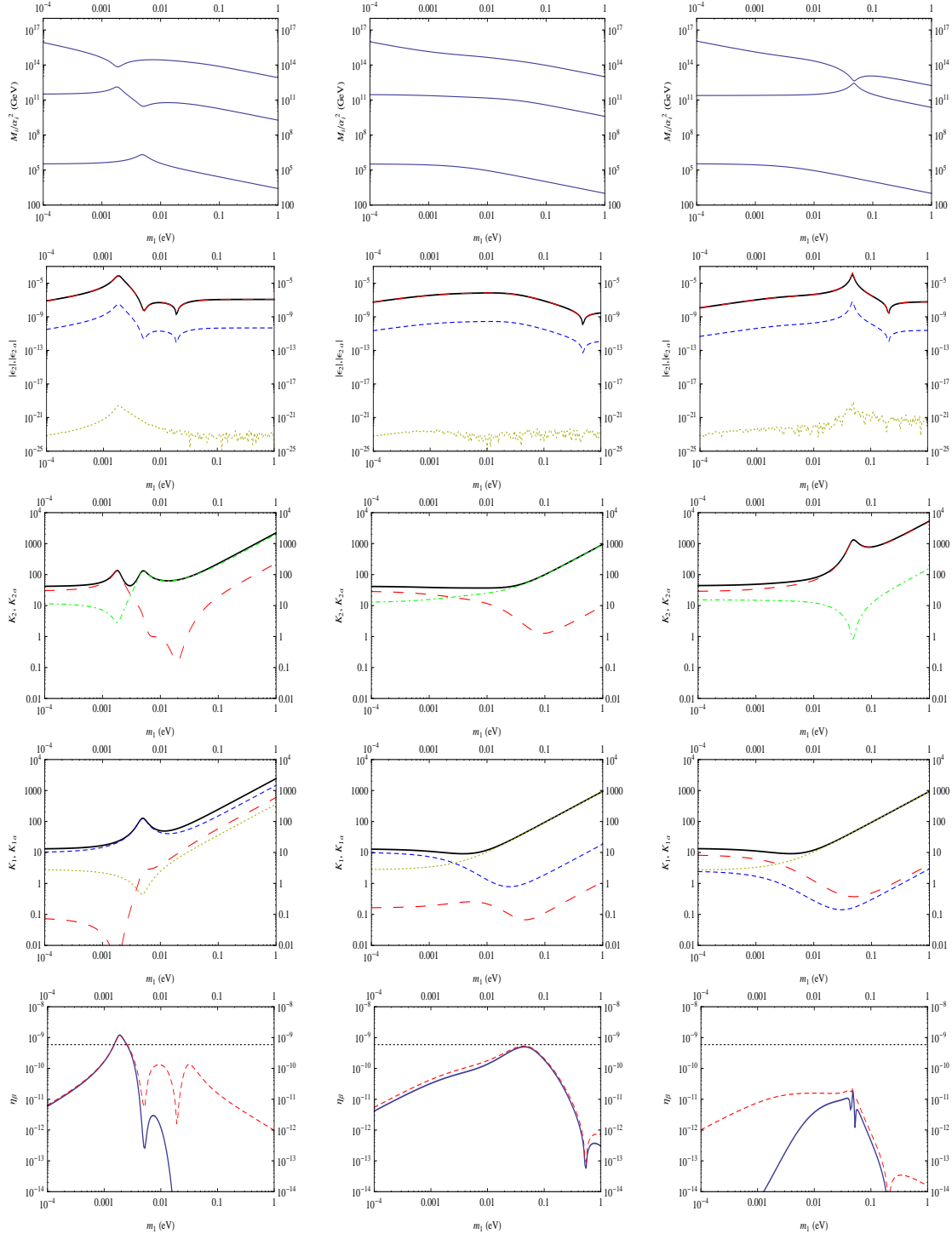


Figure 1: Case $V_L = I$, NO. Plots of the relevant quantities for three choices of the involved parameters as in Fig. 4 of Ref. [9]: $\theta_{13} = 5^\circ, \theta_{23} = 40^\circ, \theta_{12} = 33.5^\circ$ in all three cases. The values of the phases are different in the three panels (radiants): $\delta = \sigma = 0, \rho = 1.5$ (left); $\delta = 5.86, \rho = \sigma = 3$ (center); $\delta = \pi/3, \rho = 0.02, \sigma = \pi/2$ (right). The long-dashed red lines correspond to $\alpha = \tau$, the dashed blue lines to $\alpha = \mu$ and the short-dashed dark yellow lines to $\alpha = e$. In the bottom panels the horizontal dotted line is the 2σ lowest value $\eta_B^{CMB} = 5.9 \times 10^{-10}$ (cf. (1)), the solid line is η_B^f while the dashed line is $\eta_B^{T \sim M_2}$.

all the necessary conditions for the independence on the initial conditions found in [23]. Notice that these conditions also enforce an efficient wash-out of a possible pre-existing asymmetry.

A scan in the space of parameters confirms that these three solutions obtained for special sets of values are actually representative of the three general kinds of solutions that come out and, therefore, the drawn conclusions apply in general.

In the panels of Figure 2 we show the results of such a scan that highlight the allowed regions in the parameter space projected on different two-parameter planes. The scatter plots have been obtained scanning the three mixing angles θ_{12}, θ_{23} and θ_{13} over the 2σ ranges eqs.(7), the three phases δ, ρ, σ over the ranges $[0, 2\pi]$ and the absolute neutrino mass scale for $m_1 < 1 \text{ eV}$. These ranges also coincide with those shown in the plots, except for m_1 where the plots are for $m_1 > 10^{-4} \text{ eV}$ simply because no allowed solutions have been found for lower values. The shown results have been obtained in two steps. A first scan of $\mathcal{O}(10^6)$ points has yielded a first determination of the allowed regions. With a second scan of additional $\mathcal{O}(5 \times 10^6)$ points, restricted to the excluded regions, we have then more robustly and sharply determined the contours of the allowed regions. Notice that these regions have no statistical significance and the random values of the parameters have been generated uniformly.

In the top left panel the three RH neutrino masses are plotted versus m_1 . We have also plotted the lower bound on the reheating temperature calculated as

$$T_{RH}^{\min} \simeq \frac{M_2}{z_B(K_{2\tau}) - 2}. \quad (30)$$

This calculation relies on the fact that in the case $V_L = I$ the solutions, as we commented, always fall in a tauon N_2 -dominated scenario. It can be seen that the lowest bound is given by $T_{RH}^{\min} \simeq 2 \times 10^{10} \text{ GeV}$ that in a supersymmetric version, if unchanged, would be marginally reconcilable with the upper bound from the gravitino problem [24]. This is another reason to extend our investigation to cases with $V_L \neq I$ in next sections.

In the top central panel we have then plotted the allowed region in the $m_1 - \theta_{13}$ plane that can be compared with an analogous figure in [9]. Here, however, we show only those points that respect the condition $\eta_B > 5.9 \times 10^{-10}$ but for 2 different values of $\alpha_2 = 4, 5$ (in [9] we were only showing points for $\alpha_2 = 5$). The (red) star represents a point found for a minimum value $\alpha_2 = 3.4$. This point basically roughly indicates where the maximum of the asymmetry occurs in the parameter space for a fixed value of α_2 . We will continue to use this convention (yellow circles for $\alpha_2 = 5$, green squares for $\alpha_2 = 4$ and red stars for minimum found α_2 value) throughout the next figures. The structure of the allowed region in the $m_1 - \theta_{13}$ plane can be understood as follows. Since $\varepsilon_{2\tau} \propto (M_2/M_3)$ and

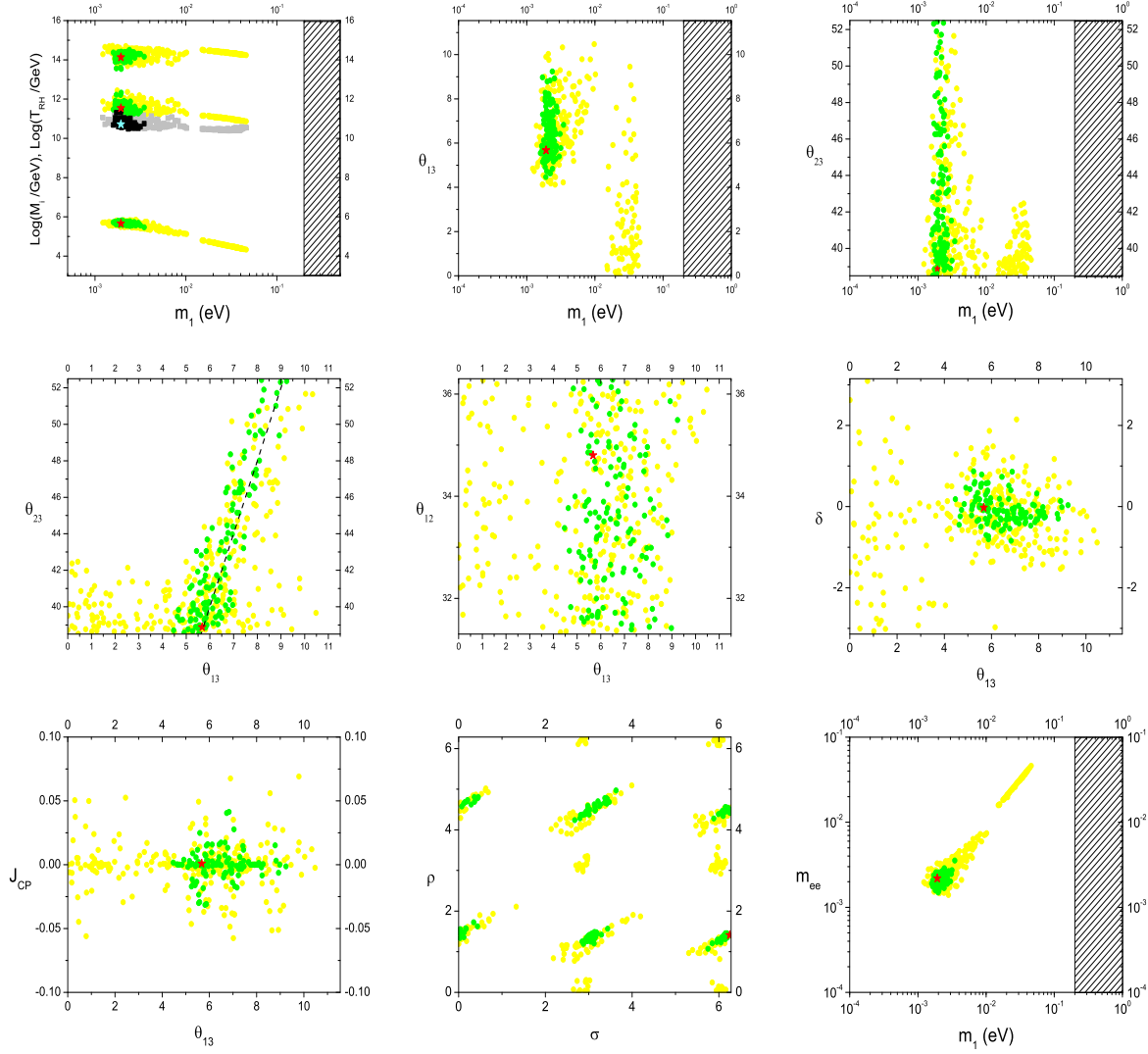


Figure 2: Case $V_L = I$, NO. Scatter plot of points in the parameter space that satisfy the condition $\eta_B > 5.9 \times 10^{-9}$ for three values of the crucial parameter α_2 : $\alpha_2 = 5$ (yellow circles); $\alpha_2 = 4$ (green circles); $\alpha_2 = 3.4$ (red stars). In the top left panel the lower bound on T_{RH} (cf. eq. (30)) is also indicated for the same values of α_2 but with different symbols: $\alpha_2 = 5$ (grey squares), $\alpha_2 = 4$ (black squares), $\alpha_2 = 3.4$ (blue star). The three mixing angles are in degrees, the three phases in radians. The dashed line in the left central panel is the eq. (34).

$M_3 \propto m_1^{-1}$, we immediately deduce that a large lepton asymmetry in the tau flavor may be produced only for sufficiently large values of m_1 . This is rather easy to understand. If m_1 tends to zero, we go into the so-called decoupling limit, $M_2/M_3 \simeq 0$. As the CP asymmetry needs (at least) two heavy states to be generated at the one-loop level, and disregarding the contribution from the N_1 , $\varepsilon_{2\tau}$ must vanish. The wash-out parameter $K_{2\tau}$ is $\mathcal{O}(25)$ [9] and therefore the final baryon asymmetry may be estimated to be

$$\eta_B \simeq 5 \times 10^{-3} \varepsilon_{2\tau} \simeq 5 \left(\frac{\alpha_2^2 m_1}{m_3} \right) \cdot 10^{-10}, \quad (31)$$

which requires

$$m_1 \gtrsim \left(\frac{5}{\alpha_2} \right)^2 10^{-3} \text{ eV}, \quad (32)$$

for NO. This estimate holds if the wash-out from the interaction with N_1 is negligible, *i.e.* $K_{1\tau} \lesssim 1$. Of course, the smaller is m_1 , the smaller $K_{1\tau}$ needs to be. For $m_1 = \mathcal{O}(10^{-3})$ eV, the only possibility is that $K_{1\tau}$ is significantly below unity. Extending the analysis of Ref. [9], one finds

$$s_{13} \cos(\delta - 2\sigma) > \frac{m_2 \tan \theta_{23}}{3\sqrt{2}m_3} \simeq 0.04. \quad (33)$$

To get the feeling of the figures involved, we may set $\delta \simeq 2\sigma$ and find that the wash-out mediated by the N_1 's vanishes for an experimentally allowed value of the mixing between the first and the third generation of LH neutrinos, $\theta_{13} > 2.3^\circ$ in agreement with our numerical results. If m_1 is larger than $\mathcal{O}(10^{-3})$ eV, then $K_{1\tau} = \mathcal{O}(1)$ is allowed and θ_{13} can be taken to be vanishing. Notice also that the lower bound eq. (33) on θ_{13} increases with $\tan \theta_{23}$. This nicely reproduces the linear dependence emerging from the numerical results in the *left column middle panel* for the plane $\theta_{13} - \theta_{23}$ and that is described, roughly for $\alpha_2 = 5$ and more accurately for $\alpha_2 = 4$, by

$$\theta_{23} \simeq 44^\circ + 4(\theta_{13} - 7^\circ), \quad (34)$$

represented with a dashed line in the panel. In the *top right panel* we show the allowed region in the plane $m_1 - \theta_{23}$.

The CP non conserving terms in neutrino oscillation probabilities can be expressed in terms of the *Jarlskog invariant* J_{CP} given by [25]

$$J_{CP} = \text{Im}[U_{\mu 3} U_{e 2} U_{\mu 2}^* U_{e 3}^*] \quad (35)$$

$$= c_{12} s_{12} c_{23} s_{23} c_{13}^2 s_{13} \sin \delta, \quad (36)$$

such that

$$P_{\nu_\alpha \rightarrow \nu_\beta} - P_{\bar{\nu}_\alpha \rightarrow \bar{\nu}_\beta} = 4 J_{CP} \sum_{k>j} s_{\alpha\beta;kj} \sin \left(\frac{\Delta m_{kj}^2 L}{2E} \right), \quad (37)$$

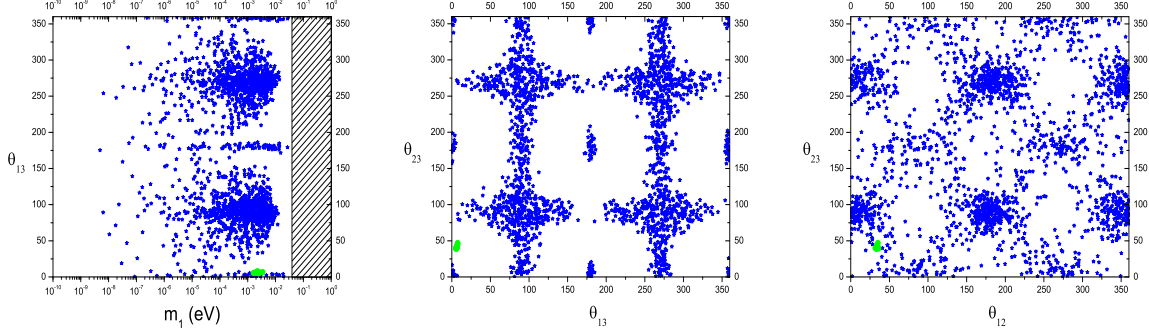


Figure 3: Case $V_L = I$, NO, $\alpha_2 = 4$. Constraints on the mixing angles obtained without imposing the current experimental information from neutrino oscillation experiments (blue points) compared to those previously obtained (green points). Notice that the regions exhibit a π periodicity and they are specular around $\pi/2$ so that all mixing angles can be limited to the physical range $[0, \pi/2]$. This can be proven to hold on very general grounds [25] and therefore this plot can be regarded as a consistency check as well.

where $s_{\alpha\beta;kj} = \pm 1$. In the bottom left panel we show the allowed points in the plane $J_{CP} - \theta_{13}$. It can be noticed that a non zero value of J_{CP} is not crucial. Looking at the bottom-central panel, it is interesting to notice that the allowed regions for the Majorana phases are centered approximately around $\sigma = n\pi$ and $\rho = (n + 1/2)\pi$.

These play a role in the determination of the *effective Majorana mass* of ν_e in $\beta\beta 0\nu$ decays that is given by

$$m_{ee} = \left| \sum_i m_i U_{ei}^2 \right| \quad (38)$$

$$= \left| m_1 c_{12}^2 c_{13}^2 e^{2i\rho} + m_2 s_{12}^2 c_{13}^2 + m_3 s_{13}^2 e^{2i(\sigma-\delta)} \right|. \quad (39)$$

In the bottom-right panel one can see how there is a precise relation between m_{ee} and m_1 , given approximately by $m_{ee} \simeq m_1$. It can be also noticed that there is quite a strict lower bound $m_{ee} \gtrsim 1.5 \times 10^{-3}$ eV. Lowest values $m_{ee} \gtrsim 2 \times 10^{-3}$ eV are the most favoured ones in this case. Though current planned experiments will not be able to test the full allowed range, it is still interesting that they will test it partially, tightening the constraints on the other parameters as well.

We have also made an interesting exercise. We determined the constraints without making use of any experimental information on the mixing angles and letting them just simply variate between 0° and 360° . The results are shown in Fig. 3. First, notice that the

lower bound on m_1 relaxes of a few orders of magnitude (see left panel). Then notice quite interestingly that small values $\theta_{13} \lesssim 10^\circ$ are well allowed for $m_1 \gtrsim 10^{-3}$ eV but values $30^\circ \gtrsim \theta_{13} \gtrsim 10^\circ$ would have been very marginally consistent. Therefore, the current bound $\theta_{13} \lesssim 10^\circ$ seems to match quite well with successful $SO(10)$ -inspired leptogenesis

On the other hand, values $\theta_{23} \lesssim 30^\circ$ would have been more optimal for $\theta_{13} \lesssim 10^\circ$ than the current experimental large atmospheric values (see the central panel in the figure). However, they are still allowed thanks to the observed range of values of the solar neutrino mixing angle (see the right panel). For the solar neutrino mixing angle there is no real favourite range of values for $\theta_{13} \lesssim 10^\circ$.

3.2 Inverted ordering

Let us now discuss the results for IO. It has been shown [26] that in grand unified models with conventional type I seesaw mechanism one can always find, for any NO model satisfying the low energy neutrino experimental constraints, a corresponding IO model. Therefore, though they exhibit some unattractive features that quite strongly disfavour them (e.g. instability under radiative corrections), IO models within grand unified theories are not unequivocally excluded. It is therefore legitimate to check whether the requirement of successful leptogenesis can somehow provide some completely independent information.

We repeated the same scan performed in the case of NO and the results are shown in figure 4, the analogous of the figure 2 for the NO case. One can see that IO is only very marginally allowed. For $\alpha_2 = 5$, there is only a small region at large values of $m_1 = (0.02 - 0.05)$ eV. Extending the analysis in Ref. [9], this is explained by the fact that the wash-out parameter $K_{1\tau}$ turns out to be

$$K_{1\tau} \simeq \frac{1}{3} \frac{(m_2 - m_1)^2}{(2m_2 + m_1)} \cdot 10^3 \text{ eV} \propto m_{\text{atm}}, \quad (40)$$

while in the NO case $K_{1\tau}$ was proportional to m_{sol} . This constrains $\varepsilon_{2\tau} \propto m_1$ to be as large as possible, thus ruling out small values of m_1 .

It is interesting to notice that in this case the allowed values for θ_{23} lie in the second octant and correspond to the largest ones compatible with the current experimental limits. The allowed values of the effective neutrino mass fall in a narrow range, $m_{ee} = (0.05 - 0.07)$ eV. Therefore, IO will be in any case fully tested from cosmology and $\beta\beta 0\nu$ experiments during next years. We will see that this conclusion will hold also allowing $V_L \neq I$. As usual, in the plots the red star corresponds to the minimum value of α_2 for which we have found a solution, $\alpha_2 = 4.65$. The corresponding set of values indicates approximately where the asymmetry has a maximum for a fixed α_2 value.

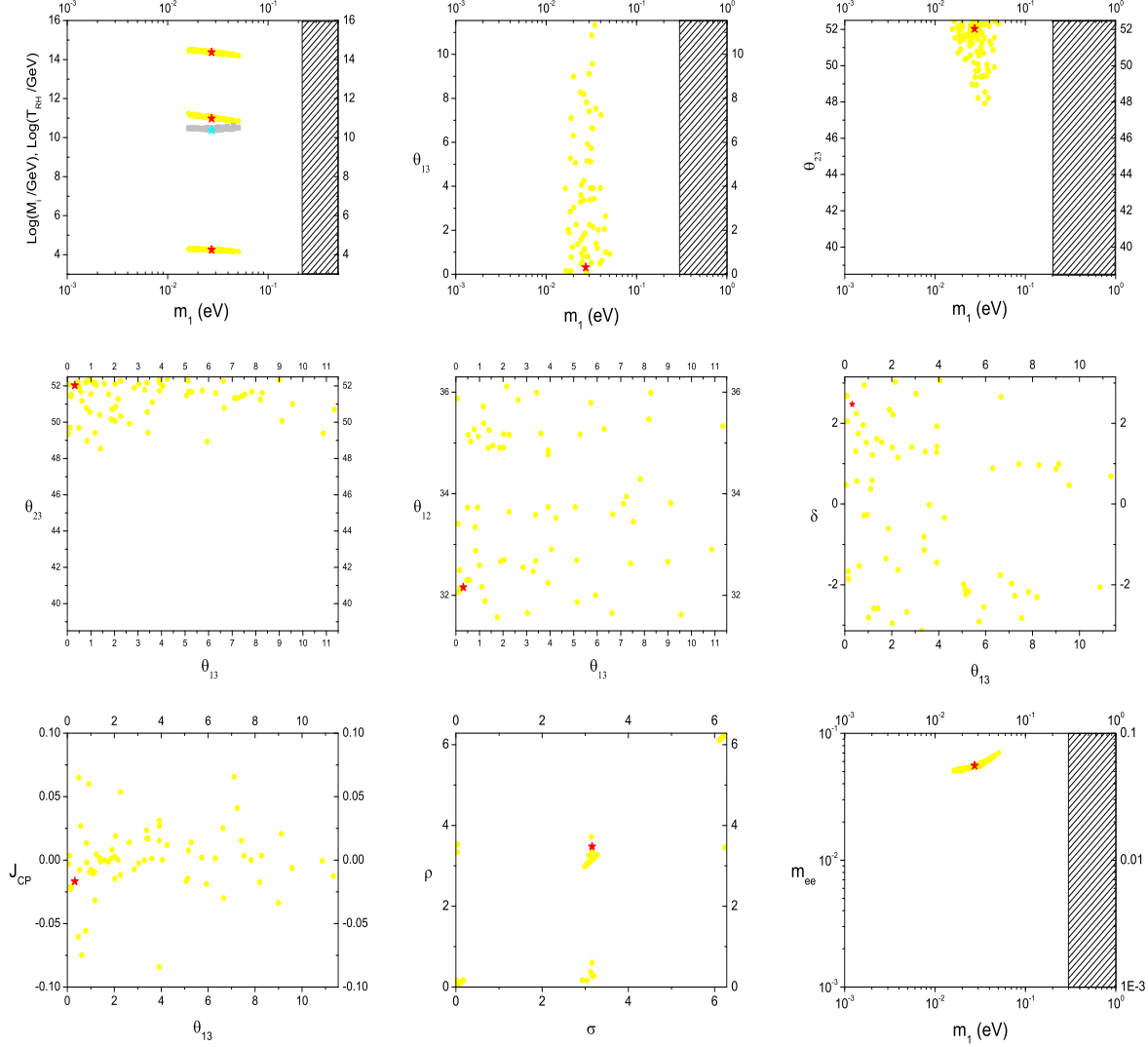


Figure 4: Case $V_L = I$, IO. Scatter plot of points in the parameter space that satisfy the condition $\eta_B > 5.9 \times 10^{-9}$ for $\alpha_2 = 5$ (yellow circles) and $\alpha_2 = 4.65$ (red star). In the top left panel the lower bound on T_{RH} (cf. eq. (30)) is also indicated for the same values of α_2 but with different symbols: $\alpha_2 = 5$ (grey squares), $\alpha_2 = 4.65$ (blue star). The three mixing angles are in degrees, the three phases in radian.

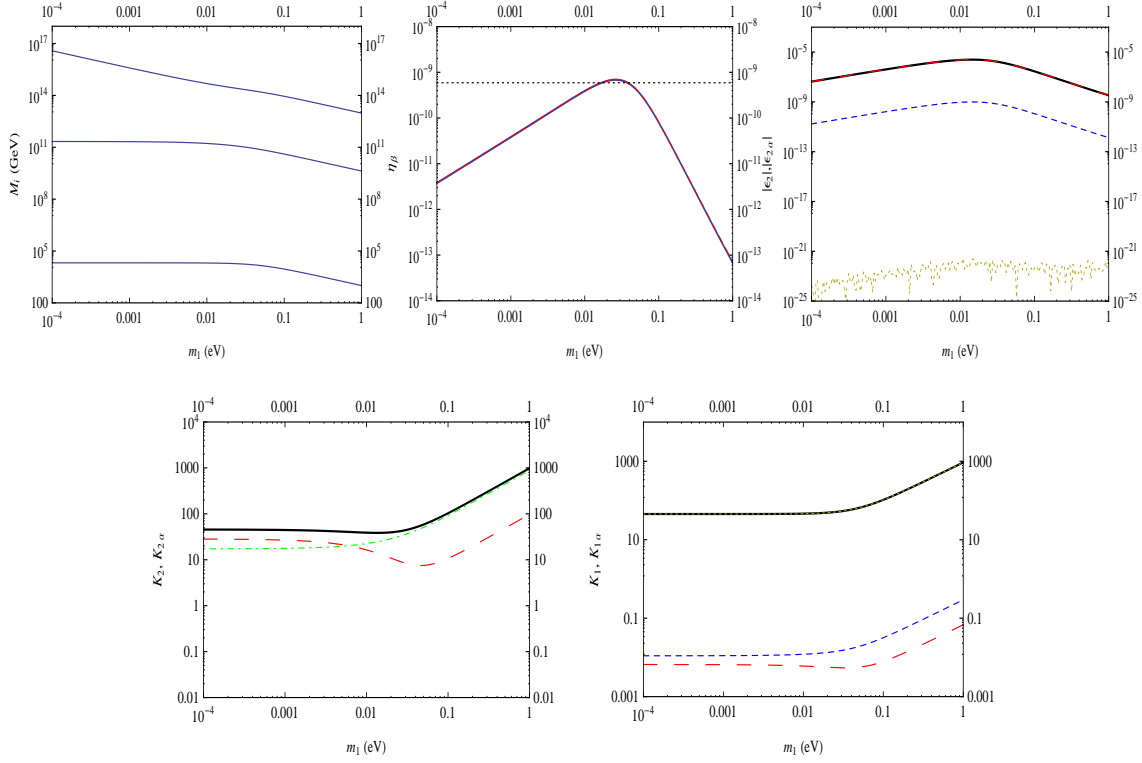


Figure 5: Case $V_L = I$, IO. Plot of all relevant quantities versus m_1 for the set of values ($\theta_{13} = 0.32^\circ, \theta_{23} = 52.03^\circ, \theta_{12} = 32.16^\circ, \rho = 3.16, \sigma = 3.48, \delta = 2.47$) corresponding to the red star in the previous figure ($\alpha_2 = 4.65$).

For this choice of values, in figure 5, we show the plots of the RH neutrino masses, of the asymmetry η_B , of the CP asymmetries $\epsilon_2, \epsilon_{2\alpha}$, of $K_1, K_{1\alpha}$ and of $K_2, K_{2\alpha}$ versus m_1 . One can see how the heaviest RH neutrino mass M_3 decreases with m_1 much faster and at $m_1 \simeq 0.001$ eV one has $M_3 \simeq 10^{17}$ GeV. Therefore, as one can see from the central top panel, the CP asymmetries are this time strongly suppressed at $m_1 \simeq 10^{-3}$ eV. On the other hand, in the range $m_1 \simeq (0.02 - 0.05)$ eV the CP asymmetries are large enough that successful leptogenesis is still possible. Notice, that this kind of solutions are a sort of modification of the solution obtained at large m_1 values for NO, simply shifted at somehow larger values. The asymmetry is therefore strongly depending on the initial conditions ($K_{2r} \simeq 1$). The first kind of solution, at small m_1 values, is completely absent.

Therefore, though IO is strongly disfavoured, it is not completely ruled out, a conclusion somehow very similar to that one obtained from completely independent arguments [26]. In this case, however, leptogenesis provides quite a precise quantitative test.

We can conclude this section saying that these results confirm and complete those

shown in [9]. In particular it is confirmed that there are viable solutions corresponding to the different points shown in the figures falling in the currently experimentally allowed ranges of the parameters. The model is therefore not ruled out. A further step is now to understand whether the model is predictive, excluding regions of the parameter space that future experiments can test. From the figures, as we have discussed, it is clear that assuming $V_L = I$ such excluded regions exist and therefore one obtains interesting constraints. However, it is important to go beyond the simple condition $V_L = I$ in order to test the stability of the constraints for variations of V_L . This is the main objective of the next sections.

4 The case $V_L = V_{CKM}$

We now study how the constraints change when a misalignment between the physical basis where m_D is diagonal and the flavour basis, where the charged lepton mass matrix is diagonal, is considered, corresponding to $V_L \neq I$. Since V_L is unitary, we can parameterize it similarly to the leptonic mixing matrix introducing three mixing angles, one Dirac-like phase and two Majorana-like phases,

$$V_L = \begin{pmatrix} c_{12}^L c_{13}^L & s_{12}^L c_{13}^L & s_{13}^L e^{-i\delta_L} \\ -s_{12}^L c_{23}^L - c_{12}^L s_{23}^L s_{13}^L e^{i\delta_L} & c_{12}^L c_{23}^L - s_{12}^L s_{23}^L s_{13}^L e^{i\delta_L} & s_{23}^L c_{13}^L \\ s_{12}^L s_{23}^L - c_{12}^L c_{23}^L s_{13}^L e^{i\delta_L} & -c_{12}^L s_{23}^L - s_{12}^L c_{23}^L s_{13}^L e^{i\delta_L} & c_{23}^L c_{13}^L \end{pmatrix} \cdot \text{diag} (e^{i\rho_L}, 1, e^{i\sigma_L}), \quad (41)$$

where we defined $s_{ij}^L \equiv \sin \theta_{ij}^L$ and $c_{ij}^L \equiv \cos \theta_{ij}^L$. Therefore, we have now six additional parameters that give much more freedom. We will not explore the full parameter space but, in the spirit of $SO(10)$ -inspired models, we will allow only small mixing angles θ_{ij}^L at the level of the mixing angles in the CKM matrix.

As a first definite example we repeat the analysis performed for the case $V_L = I$ for a definite case where the θ_{ij}^L are exactly equal to the mixing angles in the CKM matrix and therefore we set $\theta_{13}^L = 0.21^\circ$, $\theta_{23}^L = 2.3^\circ$, $\theta_{12}^L = 13^\circ$, where the latter is the measured value of the Cabibbo angle.

4.1 Normal ordering

For NO the results are shown in Figure 6. There is a first result to highlight: α_2 values as low as $\alpha_2 = 1$ are now allowed. This is an interesting result in connection with the study of realistic $SO(10)$ models. At the same time this result also implies slightly lower values of M_2 and consequentially of the minimum value of T_{reh} that can be now as low as

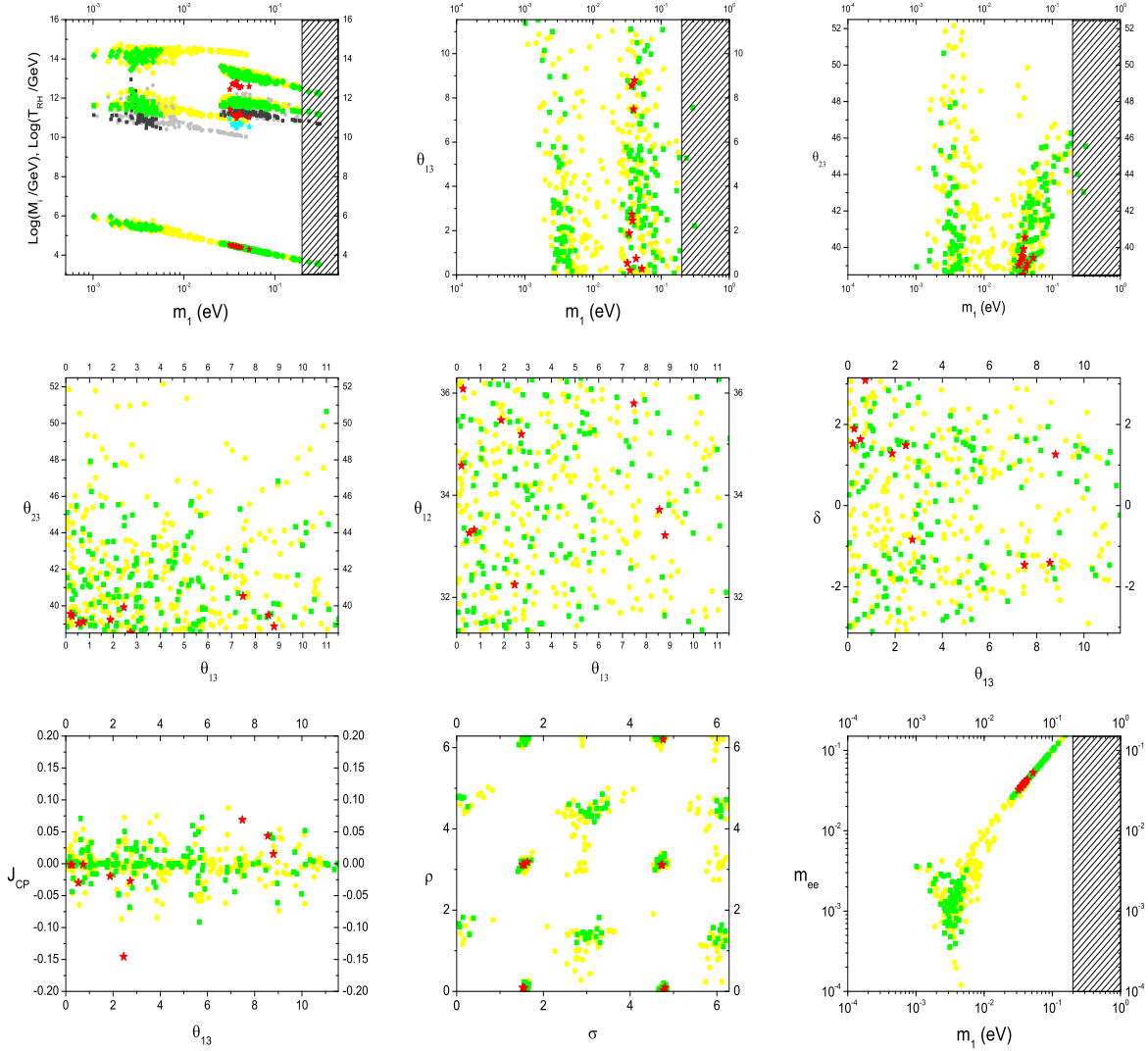


Figure 6: Case $V_L = V_{CKM}$, NO. Scatter plot of points in the parameter space that satisfy the condition $\eta_B > 5.9 \times 10^{-9}$ for $\alpha_2 = 5$ (yellow circles), $\alpha_2 = 4$ (green squares) and $\alpha_2 = 1$ (red stars). In the top-left panel, the same convention of Fig. 2 is adopted to indicate T_{RH} .

$\simeq 10^{10}$ GeV, as it can be noticed in the top-left panel in Fig. 6. In this case we have more generally calculated the minimum reheat temperature as

$$T_{RH}^{\min} \simeq \min \left[\frac{M_2}{z_B(K_{2\tau}) - 2}, \frac{M_2}{z_B(K_{2e+\mu}) - 2} \right], \quad (42)$$

considering that in the case the asymmetry at the production can be either tauon dominated or $e + \mu$ dominated. This is because the third kind of solution that was highly suppressed in the case $V_L = I$, the right panel in Fig. 1, becomes now viable and is $e + \mu$ dominated, as we will discuss soon in more detail.

Notice that if we compare the allowed points for $\alpha_2 = 4$ with those found for $V_L = I$, the constraints on the low energy neutrino parameters are now less stringent. In particular an allowed region for values $m_1 \simeq 0.003$ eV is also found for very small values of θ_{13} . Indeed, in the case $V_L = I$, and for small values of m_1 , the suppression of the wash out value $K_{1\tau}$ imposed a lower bound on θ_{13} . By choosing $V_L = V_{CKM}$ introduces the possibility of getting vanishing $K_{1\tau}$ even for zero θ_{13} angles. Extending the analysis of Ref. [9], one finds indeed that one configuration where $K_{1\tau}$ is smaller than unity is attained if $\rho = 0 \pmod{2\pi}$ and $\cos \sigma = -[1/(12 \theta_{12}^L)] [m_{\text{sol}}^4/(m_2^3 m_3)] \sim -(5/12)(m_{\text{sol}}/m_{\text{atm}}) \sim -10^{-1}$. This implies $\sigma \simeq \pi/2 \pmod{2\pi}$, as confirmed by our numerical results. Including in the analysis the atmospheric neutrino mixing angle, as one can see from the panel with the constraints in the $\theta_{13}-\theta_{23}$ plane, only values $\theta_{23} \lesssim 48^\circ$ for $\theta_{13} \lesssim 10^\circ$ are allowed for $\alpha_2 \lesssim 4$. Notice that, for $\alpha_2 \leq 4$, the allowed region in $m_1, \theta_{13}, \theta_{23}$ only marginally overlaps, at small values of θ_{23} , with the region for the case $V_L = I$. This means that a measurement of these three quantities can distinguish between the two cases, $V_L = I$ and $V_L = V_{CKM}$, and not all combinations of these three quantities seem to be possible. We will be back on this point in the next section.

In Figure 7 we plotted the relevant quantities for three particular choices of the parameters, as indicated in the figure caption, corresponding to the three kinds of solutions found for $V_L = V_{CKM}$. These three sets of values correspond to the three kinds of solutions that are found in the scan plots. The first two sets, corresponding to the left and central panels, give a tauon dominated asymmetry, while the third set, corresponding to the right panels, yields a muon dominated asymmetry. Notice that these three kinds of solutions are the same three kinds, with slight modifications, found for the case $V_L = I$. However, one can see that this time the third kind of solution, where the final asymmetry is muon dominated, also yields successful leptogenesis. The major difference that explains this result, is that for $V_L = V_{CKM}$ the flavoured CP asymmetries $\varepsilon_{2\alpha}$ are not as hierarchical as in the case $V_L = I$, as it can be clearly seen in the three panels showing the CP asymmetries in Figure 7.

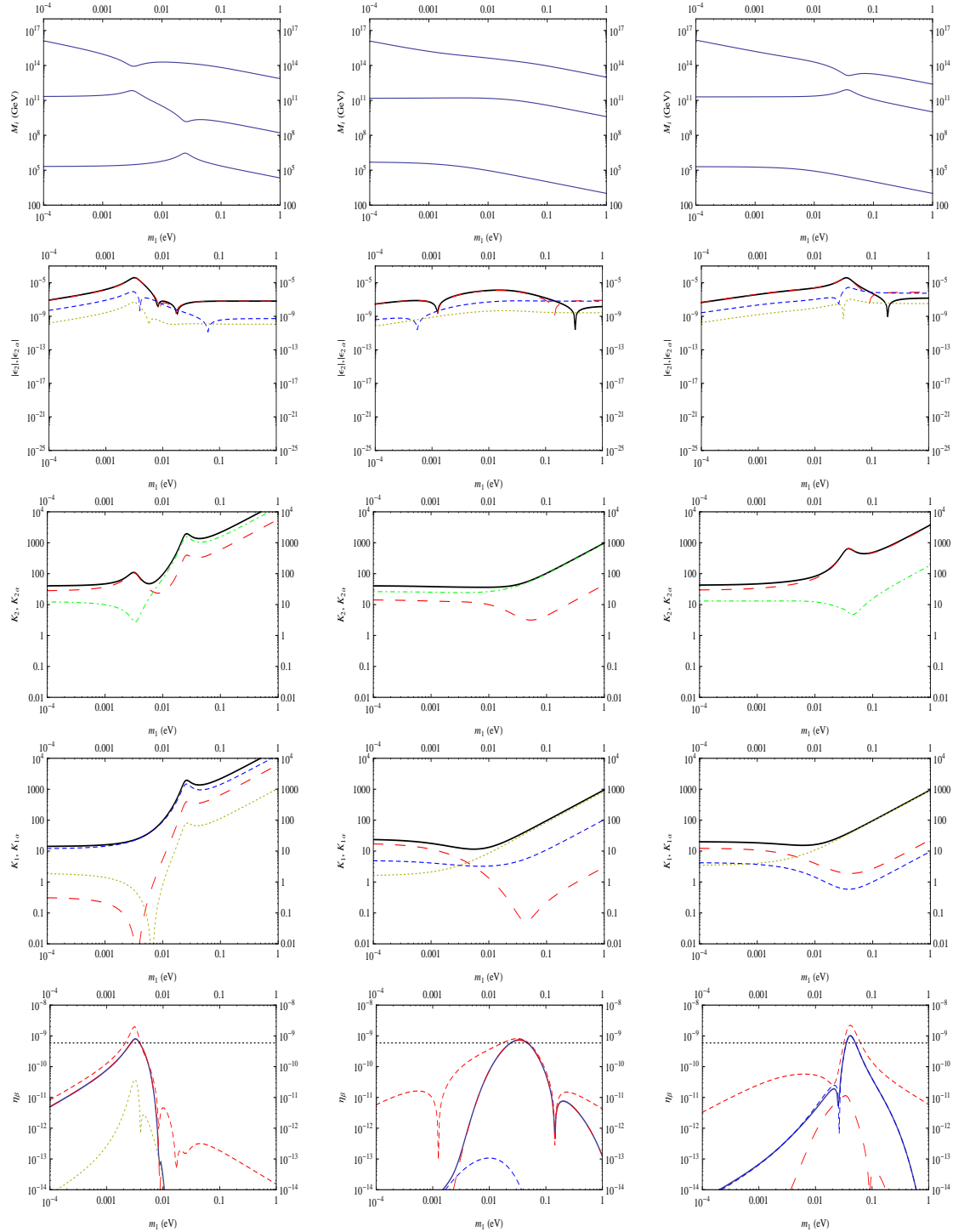


Figure 7: Case $V_L = V_{CKM}$, NO. Plots of the relevant quantities for three choices of the involved parameters. The long-dashed red lines correspond to $\alpha = \tau$, the dashed blue lines to $\alpha = \mu$ and the short-dashed dark yellow lines to $\alpha = e$. Left panels: $\alpha_2 = 4$, $\theta_{13} = 1.7^\circ$, $\theta_{12} = 33.6^\circ$, $\theta_{23} = 41.8^\circ$, $\delta = 2.84$, $\rho = 1.53$, $\sigma = 3.24$, $\rho_L = 0.12$, $\sigma_L = 2.56$; central panels: $\alpha_2 = 5$, $\theta_{13} = 3.3^\circ$, $\theta_{12} = 35.6^\circ$, $\theta_{23} = 40.4^\circ$, $\delta = -1.06$, $\rho = 2.87$, $\sigma = 6.0$, $\rho_L = 3.13$, $\sigma_L = 3.25$; right panels: $\alpha_2 = 4$, $\theta_{13} = 4.7^\circ$, $\theta_{12} = 35.9^\circ$, $\theta_{23} = 40.3^\circ$, $\delta = -1.89$, $\rho = 0.065$, $\sigma = 4.85$, $\rho_L = 5.89$, $\sigma_L = 3.69$.

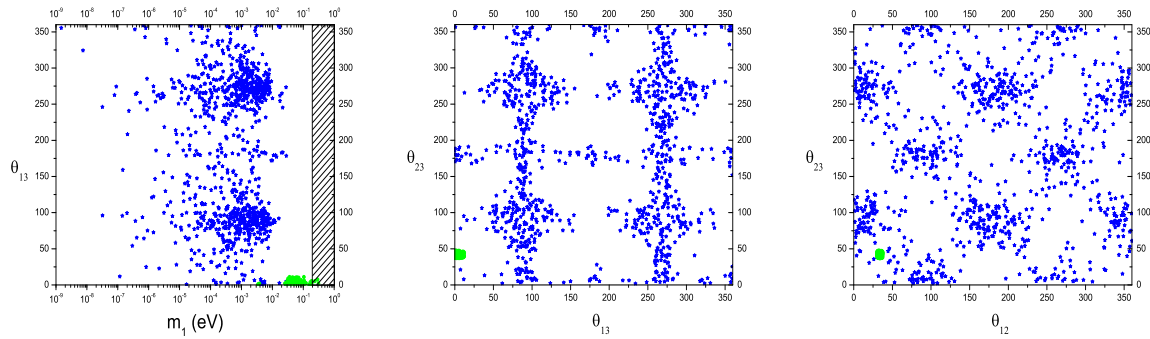


Figure 8: Case $V_L = V_{CKM}$, NO. Constraints on the mixing angles without making use of the current experimental information from neutrino oscillation experiments.

We have also repeated, as for the case $V_L = I$, the exercise to leave the mixing angles completely free, without imposing any experimental constraint finding the results shown in Fig. 8. One can see that in this case the points found when the current experimental constraints are imposed (the green points) fall in more marginally allowed regions, also for θ_{13} . This might suggest that $V_L = I$ seems to be a more attractive case than $V_L = V_{CKM}$.

4.2 Inverted ordering

Finally, we also present in Figure 9 the constraints obtained for IO. Even though there is again a remarkable suppression of the allowed regions compared to NO, they are somehow less restrictive than for $V_L = I$. In particular now a broader range of values for m_1 is allowed and θ_{23} can be as low as $\simeq 45^\circ$ for $\alpha_2 \leq 4$. This is also confirmed by the fact that lowest allowed value is now $\alpha_2 = 2$, much lower than in the case $V_L = I$ (it was $\alpha_2 = 4.65$). However, it is still fair to say that the IO case is only marginally allowed and certainly disfavoured compared to the NO case.

5 Global scans

The two specific cases that we discussed, $V_L = I$ and $V_L = V_{CKM}$, suggest an interesting sensitivity of $SO(10)$ -inspired leptogenesis to slight deviations of V_L from the identity. This sensitivity was absent in the results found in N_1 -dominated leptogenesis [5]. In this way it seems that one could even gain some information on V_L from low energy neutrino experiments. However, there is a potentially dangerous aspect of such a sensitivity: if for a slight variation of V_L the entire space of low energy neutrino parameters becomes

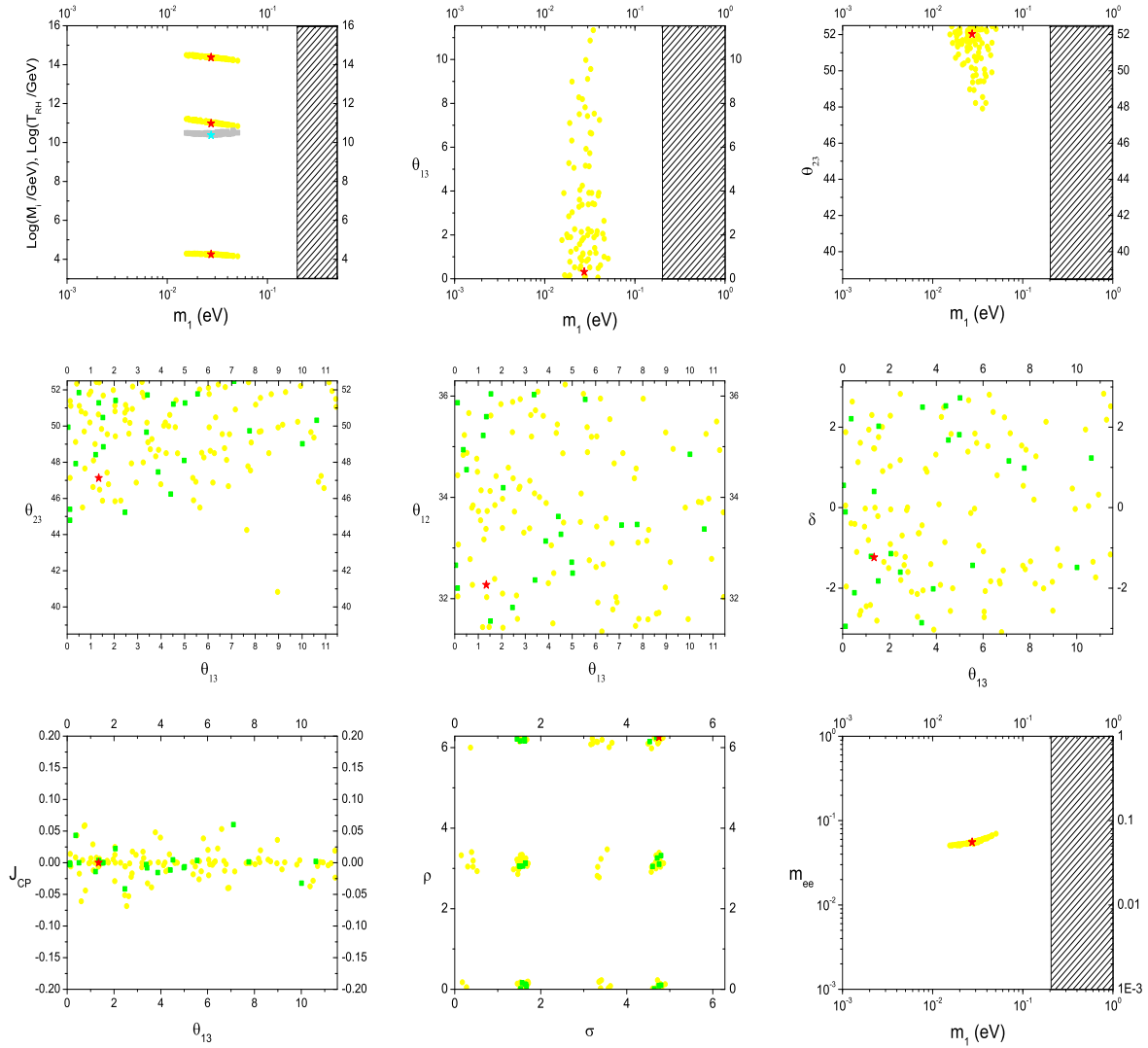


Figure 9: Case $V_L = V_{CKM}$, IO. Scatter plot of points in the parameter space that satisfy the condition $\eta_B > 5.9 \times 10^{-9}$ for $\alpha_2 = 5$ (yellow circles), $\alpha_2 = 4$ (green squares) and $\alpha_2 = 2$ (red star).

accessible, then any chance to test $SO(10)$ -inspired leptogenesis is lost. On the other hand, from a comparison of the results obtained for the two definite cases, $V_L = I$ and $V_L = V_{CKM}$, one can understand that this does not happen.

One can still suspect that for a continuous variation of the parameters in V_L , such that V_L changes from $V_L = I$ to $V_L = V_{CKM}$, new solutions appear so that any point in the space of the low energy neutrino parameters can be obtained for a proper choice of V_L .

In this section we study this issue. We perform a global continuous scan of the parameters for V_L between $V_L = I$ and $V_L = V_{CKM}$. Obviously a precise limit $V_L = V_{CKM}$ for such a global scan is somehow arbitrary. It should be therefore taken as a working assumption defining $SO(10)$ -inspired leptogenesis, even more than the condition $\alpha_i = \mathcal{O}(1)$ that, as we stressed many times, should not be regarded as a very restrictive assumption. Clearly within well defined realistic $SO(10)$ models, more specific conditions on V_L should be obtained. In any case one expects that if the V_L satisfies the condition $I \leq V_L \leq V_{CKM}$, then the allowed values for the low energy parameters should fall in the allowed regions for $SO(10)$ -inspired leptogenesis.

Therefore, in this Section we present the constraints on the low energy neutrino parameters for a continuous variation of the values of the mixing angles θ_{ij}^L in the range $0 \leq \theta_{ij}^L \leq \theta_{ij}^{CKM}$ (i.e. for $I \leq V_L \leq V_{CKM}$). More explicitly the shown scatter plots are obtained for the low energy neutrino parameters scanned over exactly the same ranges as for the case $V_L = I$. The three angles in V_L are scanned over the ranges $0 \leq \theta_{13}^L \leq 0.2^\circ$, $0 \leq \theta_{13}^L \leq 2.5^\circ$, $0 \leq \theta_{12}^L \leq 13^\circ$, while the three phases are scanned over $[0, 2\pi]$. In order to determine the allowed regions, we have followed the same strategy as in the case $V_L = I$, with a similar total number of scanned points, $\mathcal{O}(10^7)$.

5.1 Normal ordering

The results for NO are shown in figure 10. One can see how the allowed regions are approximately given by a super-position of those found for $V_L = I$ and $V_L = V_{CKM}$ plus all intermediate solutions. The result is that now the correlations among the parameters found in the two special cases seem to disappear. There are however still interesting non trivial constraints. What clearly survives is that the allowed points still cluster within two distinguished ranges of values for m_1 , one range at small values, $m_1 \simeq (1 - 5) \times 10^{-3}$ eV, and one range at high values, $m_1 \simeq 0.03 - 0.1$ eV, a distinction that is sharp for $\alpha_2 = 4$ (green squares) while it is softer for $\alpha_2 = 5$ (yellow circles). At the same time one can see that a global scan actually shows a slight correlation between m_1 and θ_{13} in the low m_1

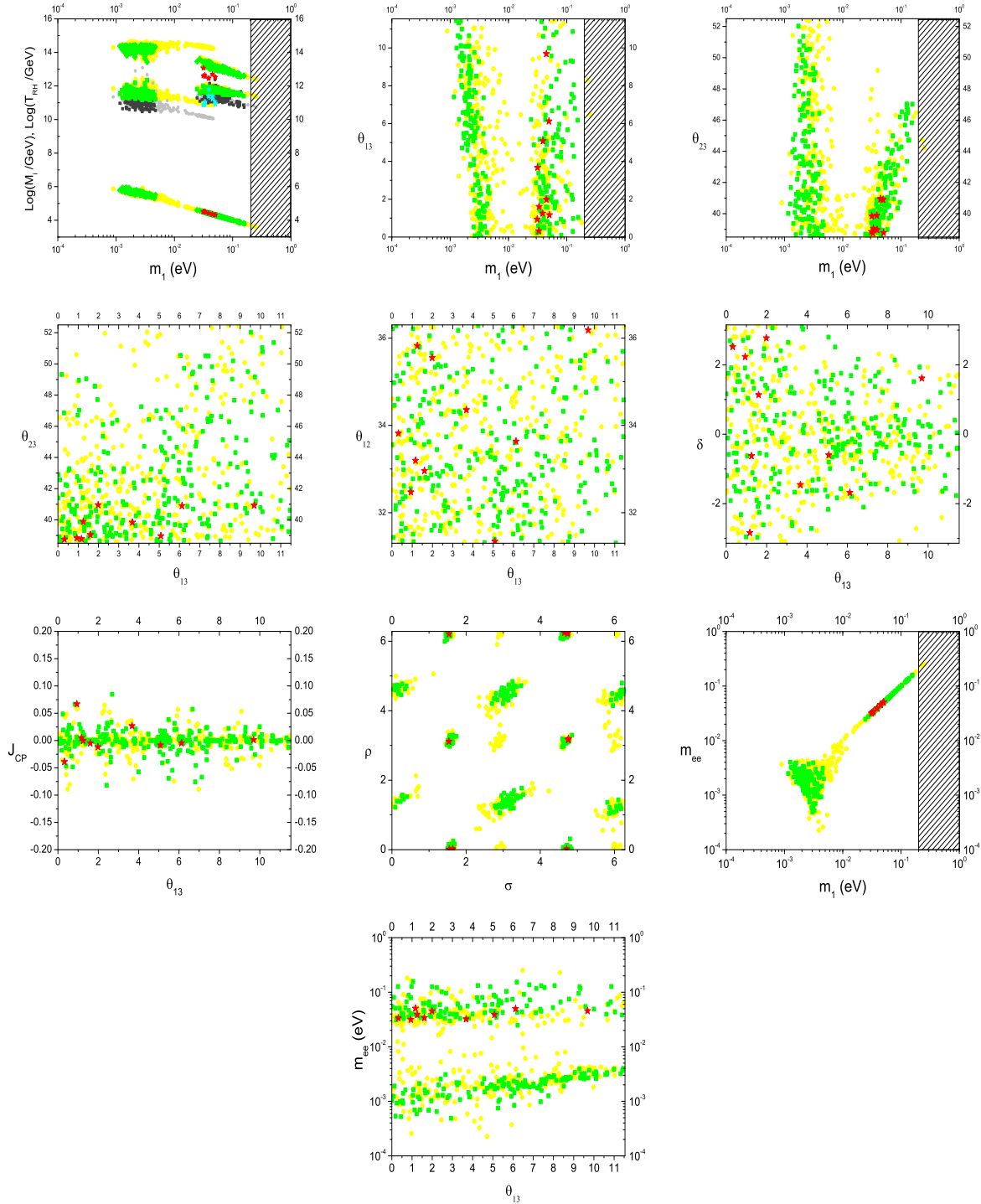


Figure 10: Global scan, NO. Scatter plot of points in the parameter space that satisfy successful leptogenesis ($\eta_B > 5.9 \times 10^{-9}$), for $\alpha_2 = 5$ (yellow circles), $\alpha_2 = 4$ (green squares) and $\alpha_2 = 1$ (red stars).

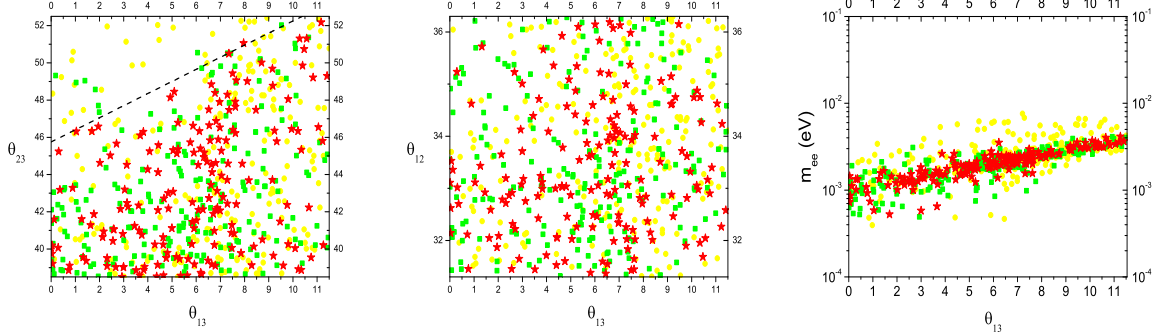


Figure 11: Global scan, NO, $m_1 < 0.01$ eV. Scatter plot of points in the parameter space that satisfy successful leptogenesis ($\eta_B > 5.9 \times 10^{-9}$), for $\alpha_2 = 5$ (yellow circles), $\alpha_2 = 4$ (green squares) and $\alpha_2 = 3.7$ (red stars). The region below the dashed line in the left panel corresponds to the condition eq. (43).

range while the interesting linear dependence between θ_{13} and θ_{23} found for $V_L = I$ seems now to be lost.

However, it should be considered that these plots are projections on two-parameters planes of an allowed region in a seven-parameter space. Therefore, only a full multi-parameters analysis would be able to unveil correlations involving more than two parameters. Nevertheless, thanks to the distinct analysis that we carried out for the two special cases $V_L = I$ and $V_L = V_{CKM}$, one can catch sight of an interesting correlation among m_1 , θ_{12} , θ_{13} and m_{ee} . To this extent, this time we have also plotted the constraints in the plane $\theta_{13} - m_{ee}$, showing how the lower bound on m_{ee} increases with θ_{13} .

5.1.1 Low m_1 range

In order to find out whether the linear dependence between θ_{13} and θ_{23} found for $V_L = I$ (cf. eq. (34)) still holds for a global scan, we show in Fig. 11 the same constraints as in Fig. 10 imposing the condition $m_1 \lesssim 0.01$ eV, since the linear dependence was found in that range of values. We only show the constraints on the relevant parameters, therefore only those in the plane $\theta_{13} - \theta_{23}$, in the plane $\theta_{12} - \theta_{13}$ and in the plane $\theta_{13} - m_{ee}$. This time we could also easily find points for $\alpha_2 = 3.7$ (red stars), showing again how allowing for a $V_L \neq I$ the allowed regions get larger.

One can see that the quite clear linear dependence eq. (34) between θ_{13} and θ_{23} holding for $V_L = I$, now turns more, for the red star points at $\alpha_2 = 3.7$, into an allowed region below the dashed line showed in the figure and corresponding approximately to

$$\theta_{23} \lesssim 49^\circ + 0.65 (\theta_{13} - 5^\circ). \quad (43)$$

This result should be also understood in terms of the condition $K_{1\tau} \lesssim 1$ (cf. (33)) when a very small V_L is allowed clearly yielding a dispersion around the linear dependence eq. (34). Notice that inside this region there are still sort of sub-regions that seem to be excluded.

We can summarize these results saying that, at low values of $m_1 \lesssim 0.01$ eV, there is an interesting testable constraints in the plane $\theta_{13} - \theta_{23}$ given by the relation eq. (43). In particular experiments that are already taking data such as the nuclear reactor experiment DOUBLE CHOOZ [27] and the long baseline experiment T2K [28] have the capability of a 3σ discovery of values $\theta_{13} \gtrsim 8^\circ$. Our results seem to suggest that if such high θ_{13} values will not be found, then a restricted range of values for θ_{23} is predicted. For example, if $\theta_{13} \lesssim 8^\circ$ then $\theta_{23} \lesssim 51^\circ$, and if $\theta_{13} \simeq 6^\circ$ then $\theta_{23} \lesssim 48^\circ$. Such a constraint on θ_{23} should be also tested during next years with quite a good accuracy by the T2K experiment [28]. These constraints in the plane $\theta_{13} - \theta_{23}$ should be considered at this level indicative, and should also consider that they are quite sensitive to the value of α_2 .

Notice that at the same time, cosmological observations and/or neutrinoless double beta decay experiments should also be able to test the condition $m_1 < 0.01$ eV. It should be therefore appreciated that this scenario will be tested during next years.

It is also interesting to notice (see right panel in Fig. 11) that there is a linear dependence between m_{ee} and θ_{13} as well. In particular, for $\alpha_2 \leq 4$, at large values $\theta_{13} \gtrsim 6^\circ$ one has $m_{ee} \simeq 10^{-3}$ eV and even for $\theta_{13} \gtrsim 8^\circ$ one has $m_{ee} \simeq 3 \times 10^{-3}$ eV. These values for m_{ee} are below the sensitivity of future planned experiments ($\gtrsim 0.01$ eV) such as EXO [29]. However, at least, m_{ee} cannot be arbitrary small but has a lower bound that, for sufficiently large θ_{13} values, is 3 times below the currently planned reachable experimental sensitivity, a very small value but maybe not completely hopeless.

Within the two-parameter analysis we are presenting, we cannot draw sharper predictions but it seems quite plausible that from a more involved multi-parameter analysis precise correlations could emerge, maybe also involving the solar neutrino angle θ_{12} . In this respect the central panel in figure 11 suggests that the solar mixing angle could indeed play also a role and that maybe sharper predictions in the 3 parameter space $(\theta_{13}, \theta_{12}, \theta_{23})$ exist.

5.1.2 Large m_1 range

We can also study how the allowed regions would reduce requiring large values $m_1 > 0.01$ eV. The results are shown in figure 12. One can see that in this case one obtains very clear constraints that will allow to test this scenario during next years in a quite

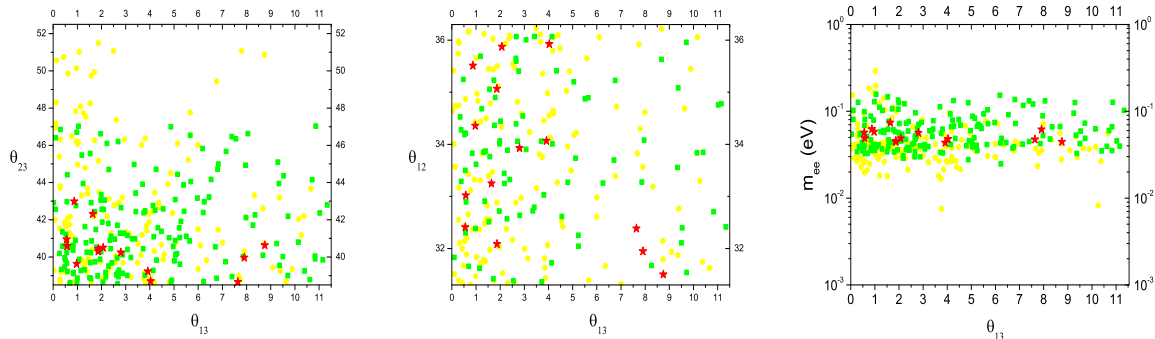


Figure 12: Global scan, NO, $m_1 > 0.01$ eV. Scatter plot of points in the parameter space that satisfy successful leptogenesis ($\eta_B > 5.9 \times 10^{-9}$), for $\alpha_2 = 5$ (yellow circles), $\alpha_2 = 4$ (green squares) and $\alpha_2 = 1$ (red stars).

unambiguous way. First of all from the Fig. 10, thanks to the very precise values of the Majorana phases, one can notice that there is a very clear relation between m_1 and m_{ee} . Second, one can see from the left panel of Fig. 12 how there is an upper bound $\theta_{23} \lesssim 46^\circ$ for $\alpha_2 \leq 4$. For values of $\theta_{13} \simeq (5-6)^\circ$, one has even $\theta_{23} \lesssim 41^\circ$. It should be said however that at these large m_1 values, one typically obtains a final asymmetry that depends on the initial conditions. Since we are assuming vanishing initial N_2 abundance and vanishing initial asymmetry, these constraints should be regarded as the most stringent ones, but likely also the best motivated ones.

5.2 Inverted ordering

Finally, we repeated the global scan for IO as well and the results are shown in Fig. 13. One can see how the allowed regions somehow merge those found for the two extreme cases $V_L = I$ and $V_L = V_{CKM}$. There is therefore nothing really new. IO is quite strongly constrained and it will be fully tested in next years. In particular we can notice again how there is a clear lower bound on θ_{23} rather than an upper bound as in NO. More particularly, one can notice that the allowed region in the plane $m_1 - \theta_{23}$ is approximately described by

$$\theta_{23} \simeq 43^\circ + 12^\circ \log(0.2 \text{ eV}/m_1) \quad (44)$$

(the dashed line in the upper right panel). It is then quite interesting that $SO(10)$ inspired leptogenesis is able to distinguish NO and IO even at $m_1 \gtrsim 0.01$ eV, when the same values of m_{ee} and of $\sum_i m_i$ (the quantity tested by cosmological observations) are found both for IO and for NO. From this point of view $SO(10)$ inspired leptogenesis provides a way to solve this ambiguity.

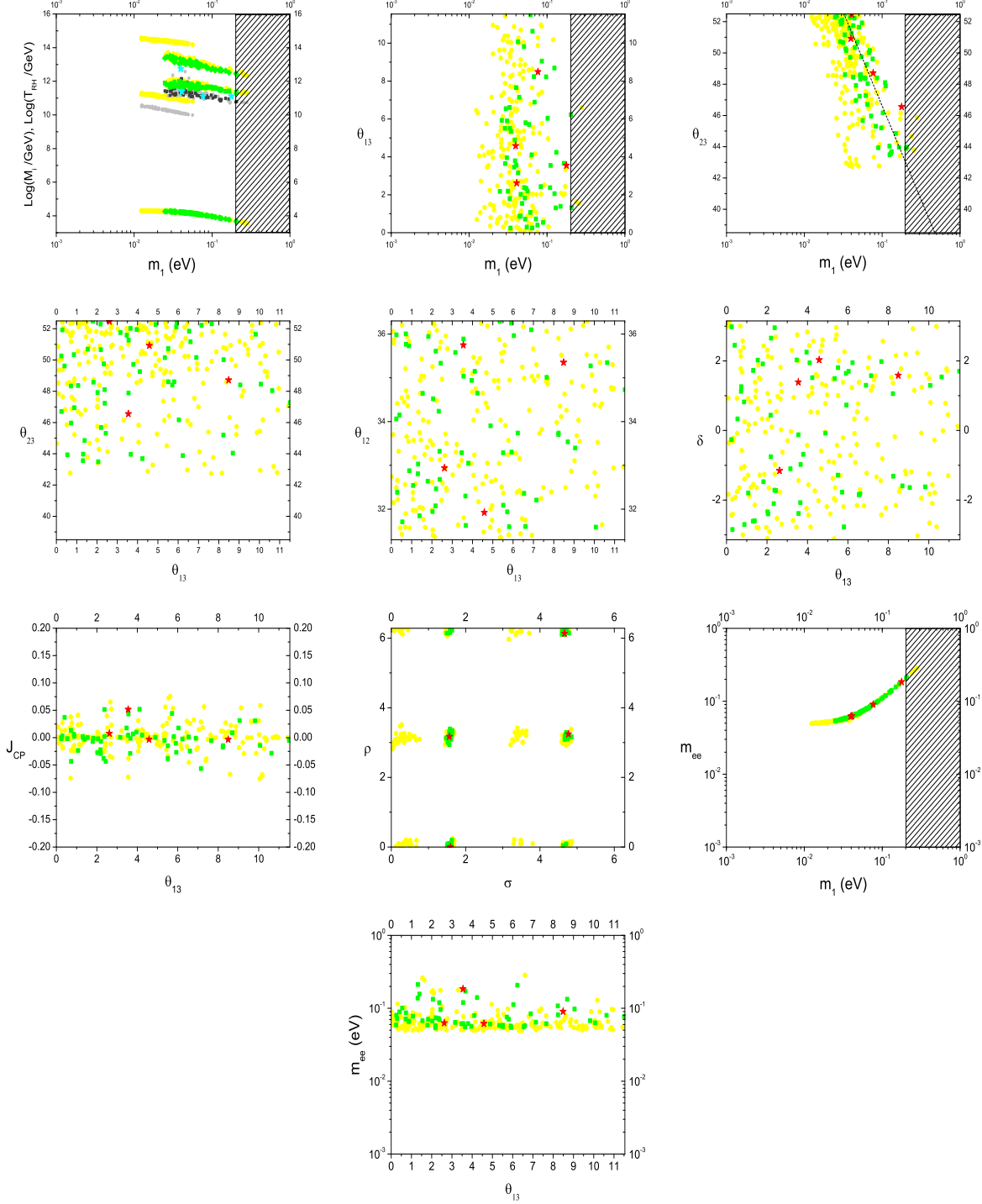


Figure 13: Global scan, IO. Scatter plot of points in the parameter space that satisfy successful leptogenesis ($\eta_B > 5.9 \times 10^{-9}$), for $\alpha_2 = 5$ (yellow circles), $\alpha_2 = 4$ (green squares) and $\alpha_2 = 1.5$ (red stars). The dashed line is the eq. (44).

6 Final remarks

We have derived constraints on the low energy neutrino parameters from $SO(10)$ -inspired leptogenesis. Our investigation shows that even minimal leptogenesis, based on a type I seesaw mechanism and assuming a thermal production of the RH neutrinos and with a traditional high mass scale RH neutrino spectrum, can be testable within a well motivated framework, where the see-saw parameter space is restricted by the $SO(10)$ -inspired conditions. The role played by the N_2 decays is crucial in this respect, not only in re-opening the viability of these models. The presence in the N_2 -dominated regime of a double stage, a production stage and a lightest RH neutrino wash-out stage, seems to introduce, as shown simultaneously both by the numerical and by the analytical results, a strong direct dependence on neutrino mixing angles as well, in addition to the dependence on the absolute neutrino mass scale, already found in usual N_1 -dominated leptogenesis [2].

Interesting predictions, that can be tested in future years, with intriguing correlations involving the absolute neutrino mass scale and the neutrino mixing angles emerge.

In the significant case of NO with low m_1 values, the neutrinoless double beta decay effective mass seems to be too small to be measured but not arbitrary small and in any case future experimental results can be anyway useful to restrict the allowed regions for the other parameters and sharpening the predictions.

The results for $V_L \neq I$ seems also to be sensitive to V_L itself and they therefore suggest that there is an opportunity to gain information on it, an interesting point within studies of specific $SO(10)$ models. It is quite interesting that there is an allowed region in the parameter space that allows large values of θ_{13} testable with on-going reactor neutrino experiments and that for these large values the models favours either large or small θ_{23} values depending whether $m_1 \lesssim 0.01$ eV or $m_1 \gtrsim 0.01$ eV.

In the small m_1 range it is also interesting that the constraints are completely independent of any assumption on the initial conditions, a point that maybe makes this option more attractive. It is actually quite interesting that this conclusion is also supported by completely independent and general considerations based on the possibility to reproduce, without a particularly fine tuned U_R matrix, the observed atmospheric to solar neutrino mass ratio, $m_{\text{atm}}/m_{\text{sol}} \simeq 6$, starting from hierarchical neutrino Yukawa couplings. It is found [30] that this experimental observation is far more natural if the lightest neutrino presents a much stronger hierarchy than the the two heavy ones, as it occurs in the region that we have found at small m_1 . It should be also stressed again, that since our results are independent of α_3 and α_1 , as far as $M_3 \gtrsim 10^{12}$ GeV and $M_1 \lesssim 10^9$ GeV, they hold even for a Yukawa couplings hierarchy milder than in the case of up quark masses. This

can help to make even more natural to reproduce the result $m_{\text{atm}}/m_{\text{sol}} \simeq 6$ without a fine tuned U_R .

A more precise measurement of θ_{12} could also play a relevant role in testing these models, a point that should be addressed by a more involved multi-parameter analysis. A future accurate determination of the neutrino mixing angles will be therefore crucial to test $SO(10)$ -inspired leptogenesis and could even yield some interesting information on the matrix V_L . In conclusion, it seems that $SO(10)$ -inspired leptogenesis provides an interesting well justified example that gives some hopes about the possibility of testing minimal leptogenesis even only with low energy neutrino experiments. It will be then quite interesting in next years to compare the experimental results with the constraints and the predictions from $SO(10)$ -inspired models that we discussed.

Acknowledgments

We wish to thank S. Blanchet, M. Chun Chen, F. Feruglio, Carlo Giunti, S. King, R. Mohapatra, M. Schmidt for useful discussions. P.D.B. acknowledges financial support from the NExT Institute and SEPnet.

References

- [1] M. Fukugita and T. Yanagida, Phys. Lett. B **174**, 45 (1986).
- [2] For a recent review, see S. Davidson, E. Nardi and Y. Nir, arXiv:0802.2962 [hep-ph]. See also, G. F. Giudice, A. Notari, M. Raidal, A. Riotto and A. Strumia Nucl. Phys. B **685**, 89 (2004); W. Buchmuller, P. Di Bari and M. Plumacher, Annals Phys. **315**, 305 (2005).
- [3] E. Komatsu *et al.*, arXiv:1001.4538 [Unknown].
- [4] P. Minkowski, Phys. Lett. B **67**, 421 (1977); M. Gell-Mann, P. Ramond and R. Slansky, *Proceedings of the Supergravity Stony Brook Workshop*, New York 1979, eds. P. Van Nieuwenhuizen and D. Freedman; T. Yanagida, *Proceedings of the Workshop on Unified Theories and Baryon Number in the Universe*, Tsukuba, Japan 1979, ed.s A. Sawada and A. Sugamoto; R. N. Mohapatra, G. Senjanovic, Phys. Rev. Lett. **44**, 912 (1980).
- [5] G. C. Branco, R. Gonzalez Felipe, F. R. Joaquim and M. N. Rebelo, Nucl. Phys. B **640**, 202 (2002).

- [6] E. Nezri and J. Orloff, JHEP **0304**, 020 (2003).
- [7] E. K. Akhmedov, M. Frigerio and A. Y. Smirnov, JHEP **0309**, 021 (2003).
- [8] S. Davidson and A. Ibarra, Phys. Lett. B **535**, 25 (2002).
- [9] P. Di Bari and A. Riotto, Physics Letters B **671** (2009) 462.
- [10] P. Di Bari, Nucl. Phys. B **727**, 318 (2005).
- [11] A. Abada, S. Davidson, F. X. Josse-Michaux, M. Losada and A. Riotto, JCAP **0604**, 004 (2006); E. Nardi, Y. Nir, E. Roulet and J. Racker, JHEP **0601**, 164 (2006); A. Abada, S. Davidson, A. Ibarra, F. X. Josse-Michaux, M. Losada and A. Riotto, JHEP **0609**, 010 (2006).
- [12] O. Vives, Phys. Rev. D **73**, 073006 (2006).
- [13] S. Blanchet, D. Marfatia and A. Mustafayev, JHEP **1011** (2010) 038 [arXiv:1006.2857 [hep-ph]]. Their analysis is restricted to normal hierarchical models with $m_1 < 0.009$ eV. Though we find agreement on some general features, for example on the existence of a lower bound on m_1 , in some cases our results seem to indicate different conclusions, like for example on the lower bound on the reheating temperature and on many features of the low energy neutrino constraints when a comparison is possible, for example we do not find a lower bound on θ_{13} when we allow $V_L \neq I$. However, it should be said that a precise understanding of the different results is made difficult because of the different framework, non supersymmetric in our case and supersymmetric in [13], and because the exact assumptions on V_L and the procedure for the calculation of U_R and of the RH neutrino mass spectrum are not specified in [13].
- [14] A. Abada, P. Hosteins, F. X. Josse-Michaux and S. Lavignac, Nucl. Phys. B **809** (2009) 183 [arXiv:0808.2058 [hep-ph]].
- [15] M. C. Gonzalez-Garcia and M. Maltoni, Phys. Rept. **460** (2008) 1; T. Schwetz, M. Tortola and J. W. F. Valle, arXiv:0808.2016 [hep-ph].
- [16] C. Amsler *et al.* [Particle Data Group], Phys. Lett. B **667**, 1 (2008).
- [17] *Matrix analysis*, Roger Horn and Charles Johnson, Cambridge University Press (1985).
- [18] S. Davidson, A. Ibarra, JHEP **0109** (2001) 013.

- [19] L. Covi, E. Roulet and F. Vissani, *Phys. Lett. B* **384**, 169 (1996).
- [20] S. Blanchet and P. Di Bari, *JCAP* **0703** (2007) 018.
- [21] S. Antusch, S. F. King and A. Riotto, *JCAP* **0611** (2006) 011.
- [22] S. Antusch, P. Di Bari, D. A. Jones and S. F. King, arXiv:1003.5132.
- [23] E. Bertuzzo, P. Di Bari and L. Marzola, arXiv:1007.1641 [hep-ph].
- [24] M. Y. Khlopov and A. D. Linde, *Phys. Lett. B* **138** (1984) 265. J. R. Ellis, J. E. Kim and D. V. Nanopoulos, *Phys. Lett. B* **145** (1984) 181; K. Kohri, T. Moroi and A. Yotsuyanagi, *Phys. Rev. D* **73** (2006) 123511.
- [25] C. Giunti and C. W. Kim, *Oxford, UK: Univ. Pr. (2007) 710 p*
- [26] C. H. Albright, *Phys. Lett. B* **599** (2004) 285.
- [27] A. Cabrera, Status of the DOUBLE CHOOZ Reactor Experiment, talk at Neutrino 2010.
- [28] T. Kobayashi, Status of T2K, talk at Neutrino 2010.
- [29] M. Dolinski, The Enriched Xenon Observatory, talk at Neutrino 2010.
- [30] J. A. Casas, A. Ibarra, F. Jimenez-Alburquerque, *JHEP* **0704** (2007) 064.